Balanced Magnetic Logic Gates in a Kagome Spin Ice

P. Gypens,[*] J. Leliaert, and B. Van Waeyenberge

Department of Solid State Sciences, Ghent University, 9000 Ghent, Belgium

Nanomagnetic logic (NML) is a promising candidate to replace or complement traditional charged-based logic devices. Single NML gates such as the three-input majority gate are well studied, and their functionality has been verified experimentally. However, such gates suffer from a problem in that they sometimes produce erroneous output when integrated into circuits. A fundamental solution is offered by using balanced logic gates: gates for which the ground states corresponding to all possible input states have the same energy. We investigate how balanced gates can be created from kagome spin ice elements. We present a balanced NAND (and NOR) gate consisting of 19 dipole-coupled uniaxially anisotropic magnets. This gate can be either driven by an external clocking field or thermally driven. In the latter case, we numerically show that the gate has a reliability of at least 96%, a number which is shown to be robust against disorder. The presented gate provides a proof of concept for an artificial kagome spin ice NML gate.

I. INTRODUCTION

Cellular automata (CA) serve as an alternative to traditional information processing paradigms. In CA, the information flow is governed by nearest-neighbor interactions between cells, while the information itself is encoded in the cell's state. Cells can be physically realized either by quantum dots which are locally linked by Coulomb interactions (QCAs) [1] or by ferromagnetic nanoislands with a single-domain magnetization (MQCAs) [2,3]. In the latter case, the information is propagated by magnetostatic stray fields. Nanomagnets of MQCAs typically have an elongated shape, such that their magnetization points along the geometrical long axis and the automaton can be used to perform binary logic operations with. These MQCAs, more commonly referred to as nanomagnetic logic (NML) systems, represent a promising candidate to replace or complement traditional charge-based logic devices due to their nonvolatility, radiation hardness, and low dissipative power losses [4].

Examples of well-studied NML architectures are wires [5–8] transmitting information from one gate to another and the three-input majority gate [9,10]. Given some boundary conditions (the input), these systems relax to their lowest energy state. This process can be either driven by an external clocking field [11,12] or thermally driven [7].

More complex NML architectures typically consist of several interconnected majority gates, and they are therefore considered circuits. These circuits can mimic the functionality of any Boolean function due to the functional completeness property of the majority gate. However, such circuits do not always yield the desired output. This is the case when the desired logic magnetization state is not equivalent to the ground state [13]. Today, circuit layout designing schemes circumvent this issue at the cost of having to completely redesign each individual circuit from scratch. To solve the problem fundamentally, a (M)QCA circuit must be built up out of *balanced* gates, gates which relax to a degenerate ground state regardless of the inputs fed into the device [14]. All NML gates proposed thus far are unbalanced, and no balanced gates have been proposed yet in the context of MQCAs.

Here, we show that a balanced NAND-NOR gate can be constructed from nanomagnets in a kagome lattice configuration, hence providing a proof of concept for an artificial kagome spin ice NML gate [15,16]. We demonstrate that this gate can operate in one of two different modes: either with the aid of an external clocking field or in a thermally driven mode (which is similar to a thermal computing one [17]). The former is tested by means of full micromagnetic simulations using the MuMax3 software package [18]. With regard to the latter, a macrospin switching model (see Sec. II) is set up to analyze the reliability of the presented gate and its robustness against disorder.

II. METHODS

We model nanomagnets made out of nickel, a magnetically soft material with the saturation magnetization $M_{sat} = 400$ kA/m. Each 11-nm-thick nanomagnet has an ellipsoidal shape with long and short axes a and b equal to 90 and 75 nm, respectively [Fig. 1(a)], thus giving them a single-domain magnetization state [2,19] described by the magnetization vector $\hat{e}_m$. The shape anisotropy dictates that the nanomagnets are magnetized preferentially

[*]Corresponding author.
Pieter.Gypens@ugent.be

(anti)parallel to their geometrical long axis **u**. These two states can be associated with logical values of 0 and 1, and both minimize the anisotropy energy

$$E_{\text{anis},i} = K_{u1}V[1 - (\hat{\mathbf{e}}_{\mathbf{m},i} \cdot \mathbf{u}_i)^2]. \quad (1)$$

In this equation, in which higher-order terms are omitted, V denotes the volume and K_{u1} the uniaxial anisotropy constant. For the size and saturation magnetization given above, the shape anisotropy is equivalent to a uniaxial anisotropy with $K_{u1} = 2936$ J/m³.

In the absence of an external clocking field, only the magnetostatic energy adds to the anisotropy energy. This contribution arises from the interaction between nanomagnets and is calculated as

$$E_{d,i} = -\mu_0 M_{\text{sat}}V(\hat{\mathbf{e}}_{\mathbf{m},i} \cdot \mathbf{H}_{d,i}), \quad (2)$$

where μ_0 is the vacuum permeability and $\mathbf{H}_{d,i}$ the point-dipole approximation of the dipolar field given by

$$\mathbf{H}_{d,i} = \frac{M_{\text{sat}}V}{4\pi} \sum_{j \neq i}^{N-1} \left[3\frac{(\hat{\mathbf{e}}_{\mathbf{m},j} \cdot \mathbf{r}_{ij})\mathbf{r}_{ij}}{r_{ij}^5} - \frac{\hat{\mathbf{e}}_{\mathbf{m},j}}{r_{ij}^3} \right]. \quad (3)$$

In this equation, N is the number of nanomagnets, $\mathbf{r}_{ij}$ is the vector pointing from nanomagnet i to nanomagnet j, and $r_{ij} = \|\mathbf{r}_{ij}\|$. In the hexagonal lattice under consideration (see Fig. 3) the nearest-neighbor distance equals 126 nm.

The energy landscape of a single nanomagnet is determined mainly by the anisotropy energy. The magnetostatic energy shifts the energy levels of these minima only slightly and leads to the formation of a local and a global minimum. The size and aspect ratio of the nanomagnets dictates that the switching process between these two states occurs through a continuous rotation of the magnetization, whereby an energy barrier ΔE has to be overcome as shown in Fig. 1(b). The same energy barrier could also be found using smaller, yet more elongated, nanomagnets. This thermally driven switching process is modeled by stochastic switching [20]. The switching time t_i of each nanomagnet [21,22],

$$t_i = -\frac{1}{f_0}\exp\left(\frac{\Delta E_i}{k_B T}\right)\ln(1 - P_i), \quad (4)$$

is determined by the attempt frequency $f_0 = 10^{12}$ Hz, the Boltzmann constant k_B, the temperature T, and a random number P_i, uniformly distributed in the interval [0,1).

The energy barrier is calculated as shown in Fig. 1(b): $\Delta E_i^{A \to B}$ is the difference between the minimum (A) and the lowest maximum between A and B. Owing to the dipolar field, the minimum (maximum) energy magnetization direction deviates slightly from the easy (hard) axis. As the switching times depend exponentially on the barrier height ΔE, we determine the exact magnetization state of these extrema with an iterative Newton-Raphson method [23], using the easy and hard axes, respectively, as initial guesses. To speed up the calculation, a look-up table is made in which the energy barriers are stored as a function of $\theta = \widehat{\mathbf{u}\mathbf{H}_d}$ and $h = (M_{\text{sat}}\mu_0 H_d/K_{u1})$. The θ value is calculated in steps of 1° in the interval [0°, 180°]. For h, the range $[10^{-4}, 10^{-1}]$ is subdivided in 1000 logarithmic steps. The upper bound on $h \approx |E_d|/E_{\text{anis}}$ is chosen such that the magnetization angle at minimum energy deviates, at most, 3° degrees from the easy axis [see Fig. 1(c)]. In this way, a switching event can safely be approximated as $\hat{\mathbf{e}}_{\mathbf{m},s} \to -\hat{\mathbf{e}}_{\mathbf{m},s}$.

The switching algorithm works in different steps. First, all nanomagnets i are initialized with the constraint that $\hat{\mathbf{e}}_{\mathbf{m},i} \cdot \mathbf{u}_i = \pm 1$. Second, the switching time for each nanomagnet is determined according to Eq. (4). Third, the nanomagnet s with the smallest switching time is switched: $\hat{\mathbf{e}}_{\mathbf{m},s} \to -\hat{\mathbf{e}}_{\mathbf{m},s}$. This switching event changes the dipolar field acting on the other nanomagnets [see Eq. (3)], and thus their energy barriers and switching times also. Therefore, it is necessary to repeat the algorithm starting from the second step in order to determine the next switching event. It is worth mentioning that the approximation $\hat{\mathbf{e}}_{\mathbf{m},s} \to -\hat{\mathbf{e}}_{\mathbf{m},s}$ allows us to determine the updated dipolar fields $\mathbf{H}_{d,i \neq s}$ by reevaluating only the term for which $j = s$ in the summation of Eq. (3). The switching
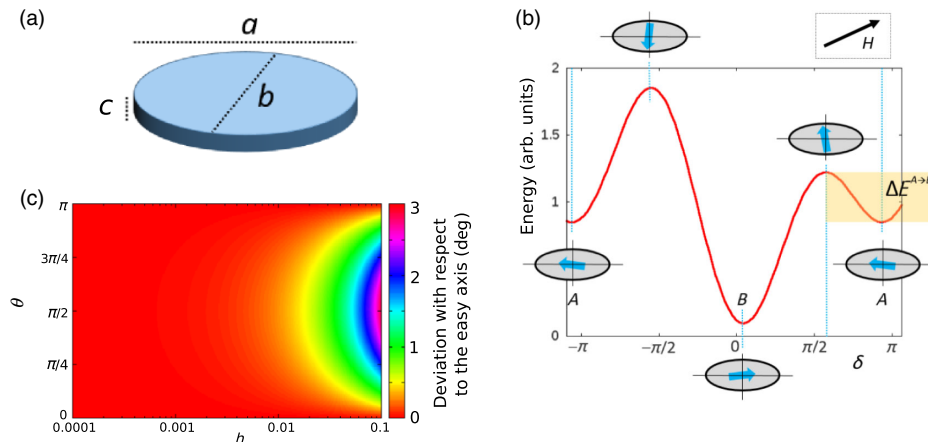

FIG. 1. (a) Nanomagnet with $a = 90$ nm, $b = 75$ nm, and $c = 11$ nm. (b) The energy landscape as a function of $\delta = \widehat{\mathbf{u}\hat{\mathbf{e}}_{\mathbf{m}}}$. The energy barrier $\Delta E^{A \to B}$ is calculated as the energy difference between the minimum (A) and the lowest maximum between A and B. The minimum (maximum) energy magnetization direction deviates slightly from the easy (hard) axis. (c) Deviation with respect to the easy axis as a function of $h = (M_{\text{sat}}\mu_0 H_d/K_{u1})$ and $\theta = \widehat{\mathbf{u}\mathbf{H}_d}$.

algorithm is stopped either after a number of switching events or when $\sum t_s$ exceeds a predefined time.

III. RESULTS

Complex nanomagnetic logic circuits are realized by connecting gates (e.g., the three-input majority gate) via wires. However, several experiments [24,25] show that the desired logic magnetization state (LS), which follows from assuming a unidirectional information flow, is not necessarily equivalent to the ground state (GS) of the circuit. As the latter dictates the functionality of NML circuits, this inequivalence may cause an erroneous output, as illustrated with an example in Figs. 2(a) and 2(b). Circuit layout designing schemes (e.g., Ref. [13]) can be used to circumvent this issue, but a more fundamental solution is to use balanced gates. Only circuits consisting of such gates function correctly [14]: balanced gates relax to a degenerate ground state regardless of the input, which implies that there is no input combination for which errors (in the wires) are energetically favorable. In other words, when the LS and the GS of the circuit are equivalent, no attention has to be paid to the circuit layout.

An almost trivial example of a balanced gate is an antiferromagnetic wire (AFMW) [5], a wirelike geometry in which the nanomagnets are placed parallel as shown in Fig. 5(a). An AFMW is balanced as it relaxes to a state having the same minimal energy for inputs 0 and 1: both inputs result in an antiferromagnetic arrangement of the nanomagnets, e.g., ↑↓↑.

We now turn our attention to the design of a balanced two input–one output gate. Throughout this article, the input magnets are depicted in green and blue, while the output magnet is marked in red. Nanomagnets that are not allowed to switch (fixed ones) are always marked in black. Experimentally, this fixation can, for example, be achieved

with the help of exchange bias [26]. The need for at least one fixed nanomagnet is dictated by the invariance under a global magnetization reversal: the total energy of the system, which scales as $(\hat{\mathbf{e}}_{\mathbf{m}})^2$, does not change when all nanomagnets are switched. Hence, the ground state associated with, e.g., input 01 and output 1 would be equivalent to the ground state associated with input 10 and output 0, as illustrated in Fig. 2(c). To avoid such a reversed output, the twofold symmetry must be broken, for instance, by introducing a symmetry-breaking fixed nanomagnet (SBFN).

Consequently, the balance condition dictates that the degeneracy of the ground state N_E has to be ≥ 8: the SBFN halves this number, and at least four states are needed to address all of the possible inputs (00, 01, 10, and 11). For simplicity reasons, we limit ourselves to $N_E = 8$ so that there are exactly four ground states left after choosing a SBFN. By "ground state," we mean the lowest energy state a gate can have given the magnetization direction of all of the fixed nanomagnets. For F fixed nanomagnets, we characterize the possible states by an array $\mathcal{A}$ having N entries (one for each nanomagnet)—with F of them being 1 or 0 and the remaining entries being free and denoted by X—e.g., $\mathcal{A} = [\mathbf{10}XX\mathbf{1}X\mathbf{0}XXXX\mathbf{1}]$. This $\mathcal{A}$ denotes 2^{N-F} states, and we use the notation $(\mathcal{A}_E)^i$ to indicate the four ground states with energy E: there are no states $\mathcal{A}_{E'}$ for which $E' < E$.

In addition to the requirement $N_E = 8$, the ground states $(\mathcal{A}_E)^i$ have to contain three nanomagnets, acting as input (underlined) and output (prime). This requirement puts a constraint on the values of the free entries, illustrated for a NAND gate below:

$$(\mathcal{A}_E)^1 = [\mathbf{10\underline{0}}X\mathbf{1}X\mathbf{0}X\underline{\mathbf{0}}X\mathbf{1}'\mathbf{1}],$$
$$(\mathcal{A}_E)^2 = [\mathbf{10\underline{0}}X\mathbf{1}X\mathbf{0}X\underline{\mathbf{1}}X\mathbf{1}'\mathbf{1}],$$
$$(\mathcal{A}_E)^3 = [\mathbf{10\underline{1}}X\mathbf{1}X\mathbf{0}X\underline{\mathbf{0}}X\mathbf{1}'\mathbf{1}],$$
$$(\mathcal{A}_E)^4 = [\mathbf{10\underline{1}}X\mathbf{1}X\mathbf{0}X\underline{\mathbf{1}}X\mathbf{0}'\mathbf{1}].$$

These two requirements form the basis of a search algorithm we develop to verify whether a geometry can be used as a balanced two input-one output gate. A geometry is defined by the positions and easy axes of all of its nanomagnets. Because the ground state has to have a degeneracy of $N_E = 8$, we focus on geometries with highly degenerate (ground) states. A well-known example is the artificial kagome spin ice [15,16], which has a honeycomb structure and for which the degeneracy arises from geometrical frustration, i.e., the inability to minimize each pairwise interaction due to the lattice topology. Indeed, four hexagons arranged as shown in Fig. 3 display the functionality of a balanced NAND gate. It consists of 19 nanomagnets, with 8 of them being fixed. The gate thus contains $2^{11} = 2048$ possible states. The energy of these states is calculated as $E = \frac{1}{2}\sum_i E_{d,i}$ (the factor $\frac{1}{2}$ is chosen to avoid double counting),
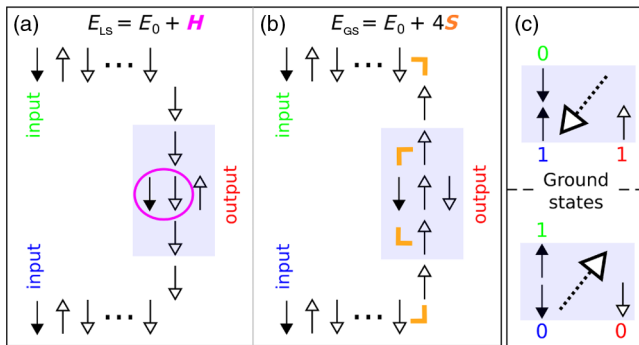

FIG. 2. (a),(b) Circuit built up out of wires and an unbalanced gate (the shaded region) producing an erroneous output: the desired logical magnetization state (a) has higher energy than the ground state (b) if $H > 4S$. Arrows with a filled arrowhead represent fixed nanomagnets. (c) Global reversal between ground states (the large arrow symbolizes the magnetization direction of all other nanomagnets).
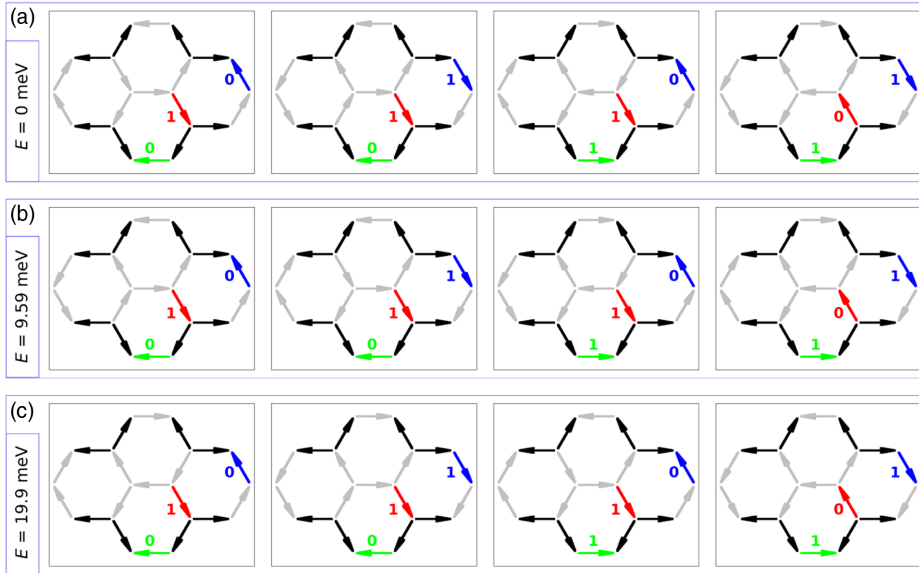
FIG. 3. The geometry consisting of 19 dipole-coupled uniaxial nanomagnets corresponding to a thermally driven, balanced NAND gate. The desired output (red) is obtained when the system is in its (a) ground state, (b) first excited state, and (c) second excited state. The energy of a state is calculated as $E = \frac{1}{2}\sum_i E_{d,i}$, using the ground-state energy as a reference. Green and blue arrows denote the input bits, while black arrows denote the fixed nanomagnets. Bit value 1 corresponds to a magnetization pointing to the right. When the magnetization direction of the fixed nanomagnets is reversed, this geometry can also be used as a NOR gate.

using the ground-state energy as a reference. We find four states having an energy of $E = 0$ meV and corresponding to the four possible inputs [see Fig. 3(a)]. This calculation demonstrates that the gate is balanced, hence providing a proof of concept for an artificial kagome spin ice NML gate. From the geometries we investigate, this is the only one suited as a balanced logic gate. An overview of all of the tested geometries is given in Fig. 4.

A. Thermally driven

An annealing procedure [27,28] is performed to ensure that the system evolves to (and remains in) the desired ground state by reducing the temperature from 600 to 120 K in steps of 5 K, each time after either 1000 s or 100 000 switching events. For the systems studied here, this cooling rate is sufficiently slow to avoid quenching. We do not claim, however, that this annealing scheme is the optimal choice. The optimization of the annealing does not lie within the of scope of our work, and the reliabilities should therefore be interpreted as lower limits.

The reliability of AFMWs is described extensively in the literature [5–8]. We repeat the general conclusions by illustrating them in Fig. 5(b). The presented results are obtained by annealing 50 AFMWs, in which the first nanomagnet is fixed in the *up* direction and the other nanomagnets have an initial random orientation (i.e., up or *down*). The final states are then compared to the desired ground state. We notice that the reliability decreases when we look at a nanomagnet farther away from the input. This reliability decrease is explained by the fact that the magnetization of each nanomagnet has a certain, yet small, probability to align parallel to its neighbor. We also corroborate that the reliability decreases when the distance
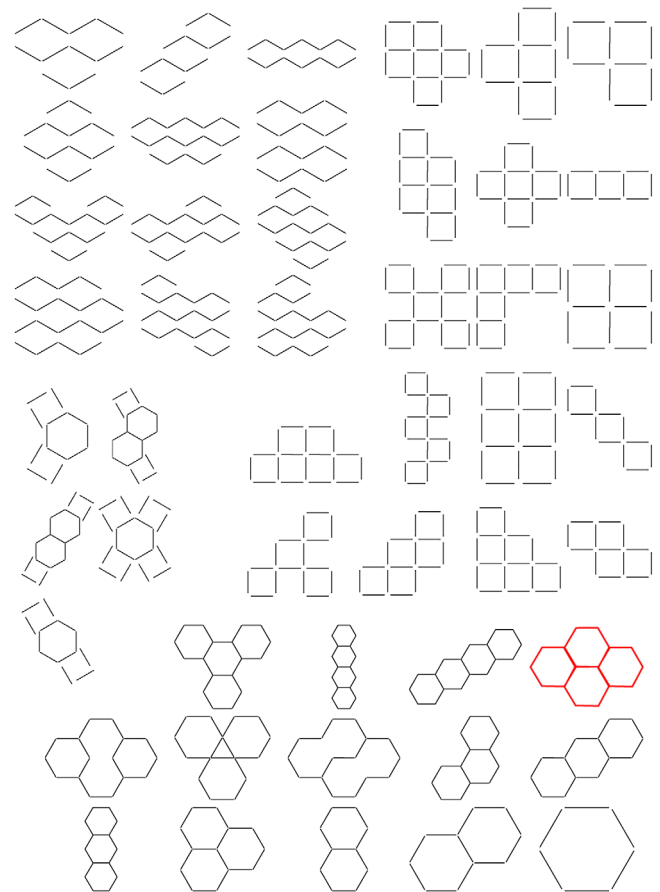

FIG. 4. An overview of all geometries tested with the search algorithm. Because of computational restrictions, only systems containing fewer than 22 nanomagnets are considered. The geometry which can be used as NAND and NOR gates is highlighted in red.
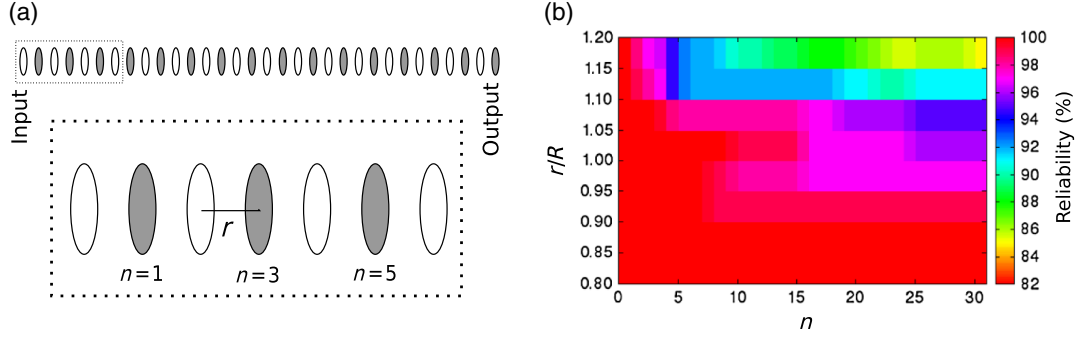
FIG. 5. (a) AFMW. (b) The reliability depends on the number of and the spacing between the wire components. The intercomponent distance r is normalized on $R = 126$ nm. The results are obtained by annealing 50 AFMWs, in which the first nanomagnet is fixed in the up direction and the other nanomagnets have an initial random orientation (i.e., up or down). The final states are then compared with the desired ground state.

between the nanomagnets increases because of the weakened magnetostatic coupling between the nanomagnets.

Similar to the reliability of the AFMW, the reliability of the presented NAND gate is tested by annealing the system 50 times for each input using the annealing scheme mentioned previously. The results are summarized in Table I and show how often the system reaches its ground state [Fig. 3(a)], and its first [Fig. 3(b)] and second excited states [Fig. 3(c)]. The last two also give rise to the desired output, resulting in a reliability of at least 96%.

Next, we investigate the robustness of the reliability against disorder. Two types of disorder are considered: the variability in the nanomagnets' (shape) anisotropy constant, and the variation in the easy-axis direction. To this end, in this set of simulations, the anisotropy constant of each nanomagnet is changed by drawing from a Gaussian distribution with standard deviations σ reaching from 1% to 9%. Subsequently, the system is relaxed 50 times for each input using the annealing scheme described earlier. This procedure is repeated ten times. The results for the worst performing inputs are shown in Fig. 6(a). The robustness towards variations in the easy-axis directions is tested in a similar manner. We consider deviations up to 5° with respect to the ideal case. The results are shown in Fig. 6(b).

TABLE I. The performance of the NAND gate shown in Fig. 3 is tested by annealing it 50 times for each input, starting with a random state. The temperature is reduced by 5 K after either $t = \sum t_s > 1000$ s or 100 000 switching events. Note that the operation speed can be increased by using nanomagnets with a lower aspect ratio or a smaller volume, as this change lowers the time scale of a typical switching event.

Input		00	01	10	11
Ground state:	Fig. 3(a)	11/50	32/50	33/50	25/50
First excited state:	Fig. 3(b)	12/50	15/50	16/50	23/50
Second excited state:	Fig. 3(c)	24/50	1/50	1/50	2/50
Other states		3/50	2/50	0/50	0/50
Desired output		100%	96%	100%	100%

The robustness of our results against disorder is checked by altering the strength and direction of the anisotropy. We do not considered disorder due to material defects inside the nanomagnets because this effect mainly plays a role in elongated nanomagnets, in which the switching occurs via the creation, propagation, and annihilation of a domain wall. In such systems, material defects could serve as nucleation centers for this domain wall.

B. Clocked operation

In this section, we demonstrate how the balanced NAND gate can operate with the aid of an external clocking field. We perform full micromagnetic simulations by using the MUMAX3 software package. The exchange stiffness and the damping constant are equal to $A_{ex} = 13 \times 10^{-12}$ J/m and $\alpha = 0.01$, respectively. The islands, being 11 nm thick and having an ellipsoidal shape with long and short axes equal to 90 and 75 nm, are discretized in cells sized $3 \times 3 \times 11$ nm. All islands are initialized perpendicular to the plane by applying a global external field of 1 T in the positive z direction. This global field is then gradually reduced to zero in small steps while we let the magnetization relax to its equilibrium configuration between each step. In the meantime, a local external field, providing a bias direction for the fixed and input nanomagnets, is increased from zero to 3.5 mT, ensuring that these nanomagnets relax to the desired state. The final magnetization states are shown in Fig. 7. Each input combination results in the correct output, although the ground states predicted in Fig. 3 are not reached.

IV. DISCUSSION

The qualitative results obtained for the NAND gate also hold when the magnetization direction of all of the fixed nanomagnets is switched. This is the case because a global reversal does not affect the energy states. On the other hand, a global reversal includes a change in the bit value of the input and the output. Replacing 0 by 1, and vice versa, in
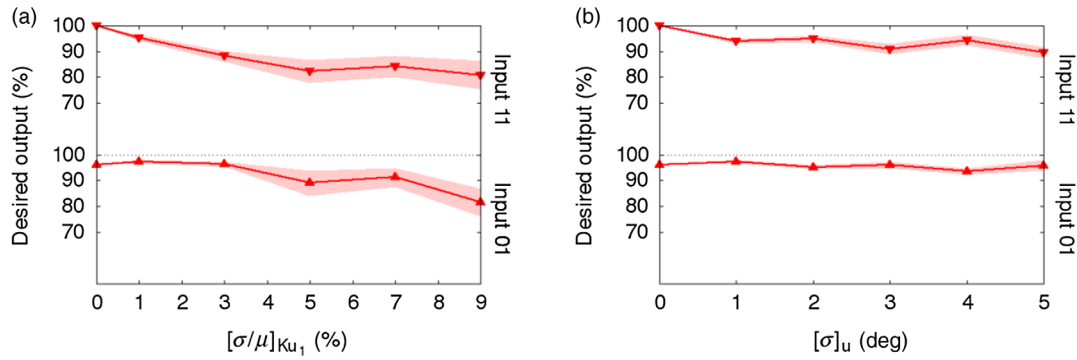
FIG. 6.   The reliability as a function of disorder strength for input 11 (top halves of the panels) and input 01 (bottom halves of the panels). The other inputs yield the desired output of 100% over the entire disorder range and are omitted for the sake of clarity. (a) The variability in the nanomagnets' (shape) anisotropy constant. (b) The variation in the easy-axis direction with respect to the ideal case. The points show the average of ten disorder realizations. The shaded regions depict the standard error.

the truth table, we recover that this operation transforms a NAND gate into a NOR gate. This insight shows that the presented geometry can be used as a NAND as well as a NOR gate, with the only difference being the magnetization direction of the fixed nanomagnets.

Our simulations show that, when the presented gate is thermally driven, the reliability of the gate is at least 96% in the absence of disorder. When we include disorder, this number decreases slightly, but it remains higher than 80% for the strongest disorder under consideration. As stated earlier, these numbers should be interpreted as lower limits since the annealing is not yet optimized. In general, slower cooling leads to higher reliability. Although this slower

cooling comes at the expense of a longer computation time, one has to take into account that the time scales inherent to thermally driven logic are much slower than the operation speed of its clocked counterpart [7,29]. Therefore, thermally driven logic should be considered only when the speed of the computation is not the main requirement [30].

Thus far, we have discussed the performance of a single gate only. The next step is to elucidate how to incorporate these balanced gates into a logic circuit. To construct more complex logic functions, one can interconnect the inputs and outputs of several gates via AFMWs. Because our gate has the property of functional completeness, any Boolean function can be realized in this way. However, certain problems arise.

First, in the case of thermally driven logic, the cooling rate should be reconsidered (i.e., lowered) to avoid quenching in a high-energy state. For larger circuits, some driving force is needed in order to ensure that the computation correctly evolves in the forward direction [17].

Second, when bringing an AFMW in the vicinity of our gate, the interplay between these two structures results in a shift of energy levels, and the balancing criterion is no longer fulfilled. For example, the outermost nanomagnet of an AFMW couples not only to the (blue) input of the
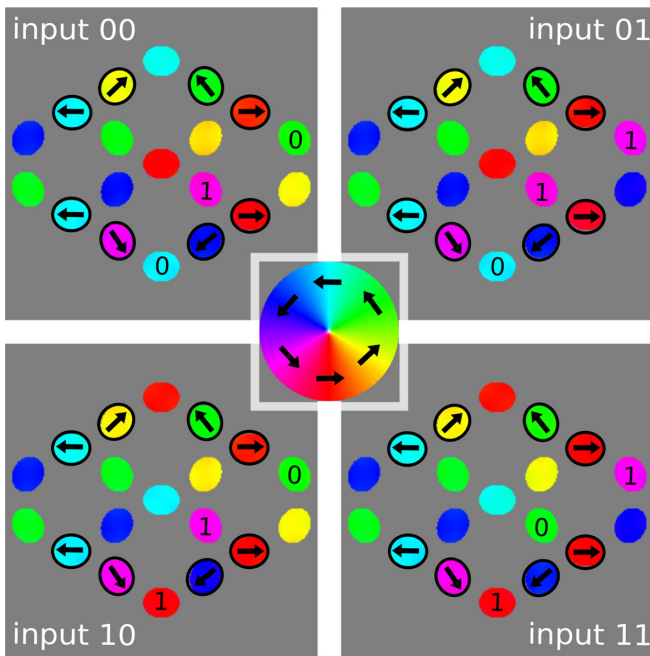

FIG. 7.   The final magnetization states obtained after the clock operation, as described in the text. The color code indicating the magnetization direction of the magnetic islands is shown in the center.
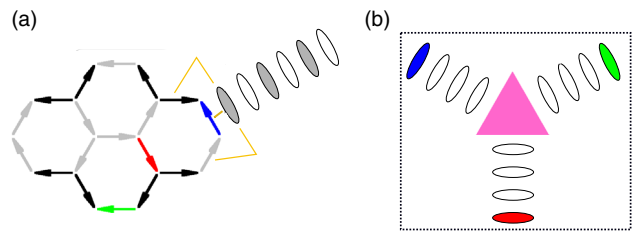

FIG. 8.   (a) The nanomagnet of an AFMW couples not only to the input of the gate but also to the nanomagnets surrounding this input (shown in yellow). (b) Schematic representation of a gate for which the inputs and outputs are located at the ends of AFMW-like arms. The triangle symbolizes a more complex geometry whose details are still unknown.

gate but also to the nanomagnets surrounding this input [Fig. 8(a)]. This effect can be avoided if the inputs and outputs of the balanced gate are located at the ends of AFMW-like "arms" [Fig. 8(b)]. In this way, the gates and wires can be treated as separated "blocks." Because of their balanced quality, we can interconnect these blocks without worrying about errors which arise in traditional NML circuits as a consequence of the difference between the desired logic state and the ground state. However, the search for a geometry like that shown in Fig. 8(b) is still ongoing.

V. CONCLUSION

To conclude, we discuss in this paper the need for balanced gates in the context of NML circuits. We present a proof of concept for a balanced NAND and NOR gate. This gate can be either driven by an external clocking field or thermally driven. For the latter case, we analyze its reliability and its robustness against disorder. The balancing criterion is fulfilled by taking advance of the geometrical frustration inherent to an artificial kagome spin ice. This frustration gives rise to a complex energy landscape consisting of multiple local energy minima separated by large energy barriers, which can only be overcome with several consecutive spin flips. In the case of thermally driven logic, this complex energy landscape necessitates an annealing procedure in order to allow the system to relax into the desired ground-state configuration. It remains to be investigated whether balanced NML gates also exist with lower energy barriers between the energy minima, allowing the system to evolve to and remain in the desired ground state at constant temperature.

ACKNOWLEDGMENTS

[1] C. S. Lent, P. D. Tougaw, W. Porod, and G. H. Bernstein, Quantum cellular automata, Nanotechnology **4**, 49 (1993).

[2] R. P. Cowburn and M. E. Welland, Room temperature magnetic quantum cellular automata, Science **287**, 1466 (2000).

[3] G. Csaba, A. Imre, G. H. Bernstein, W. Porod, and V. Metlushko, Nanocomputing by field-coupled nanomagnets, IEEE Trans. Nanotechnol. **1**, 209 (2002).

[4] G. Csaba, P. Lugli, and W. Porod, in *Proceedings of the 4th IEEE Conference on Nanotechnology, Munich, 2004* (IEEE, New York, 2004), p. 346.

[5] R. P. Cowburn, Probing antiferromagnetic coupling between nanomagnets, Phys. Rev. B **65**, 092409 (2002).

[6] J. F. Pulecio, P. K. Pendru, A. Kumari, and S. Bhanja, Magnetic cellular automata wire architectures, IEEE Trans. Nanotechnol. **10**, 1243 (2011).

[7] D. B. Carlton, B. Lambson, A. Scholl, A. T. Young, S. D. Dhuey, P. D. Ashby, E. Tuchfeld, and J. Bokor, Computing in thermal equilibrium with dipole-coupled nanomagnets, IEEE Trans. Nanotechnol. **10**, 1401 (2011).

[8] Z. Gu, M. E. Nowakowski, D. B. Carlton, R. Storz, M.-Y. Im, J. Hong, W. Chao, B. Lambson, P. Bennett, M. T. Alam *et al.*, Sub-nanosecond signal propagation in anisotropy-engineered nanomagnetic logic chains, Nat. Commun. **6**, 6466 (2015).

[9] G. Csaba, A. Imre, G. Bernstein, W. Porod, and V. Metlushko, in *Proceedings of the 2002 2nd IEEE Conference on Nanotechnology, Washington, DC, 2002* (IEEE, New York, 2002), p. 59.

[10] A. Imre, G. Csaba, L. Ji, A. Orlov, G. Bernstein, and W. Porod, Majority logic gate for magnetic quantum-dot cellular automata, Science **311**, 205 (2006).

[11] M. Niemier, M. Alam, X. S. Hu, G. Bernstein, W. Porod, M. Putney, and J. DeAngelis, in *Proceedings of the 2007 International Symposium on Low Power Electronics and Design, Portland, OR, 2007* (Association for Computing Machinery, New York, 2007), p. 26.

[12] E. Varga, G. Csaba, G. Bernstein, and W. Porod, Domain-wall assisted switching of single-domain nanomagnets, IEEE Trans. Magn. **48**, 3563 (2012).

[13] S. Liu, G. Csaba, X. S. Hu, E. Varga, M. T. Niemier, G. H. Bernstein, and W. Porod, in *Proceedings of the 50th Annual Design Automation Conference, Austin, 2013* (Association for Computing Machinery, New York, 2013), p. 106.

[14] J. C. Lusth and B. Dixon, A characterization of important algorithms for quantum-dot cellular automata, Information Sciences (NY) **113**, 193 (1999).

[15] Y. Qi, T. Brintlinger, and J. Cumings, Direct observation of the ice rule in an artificial kagome spin ice, Phys. Rev. B **77**, 094418 (2008).

[16] N. Rougemaille, F. Montaigne, B. Canals, A. Duluard, D. Lacour, M. Hehn, R. Belkhou, O. Fruchart, S. El Moussaoui, A. Bendounan, and F. Maccherozzi, Artificial Kagome Arrays of Nanomagnets: A Frozen Dipolar Spin Ice, Phys. Rev. Lett. **106**, 057209 (2011).

[17] C. H. Bennett, The thermodynamics of computation—A review, Int. J. Theor. Phys. **21**, 905 (1982).

[18] A. Vansteenkiste, J. Leliaert, M. Dvornik, M. Helsen, F. Garcia-Sanchez, and B. Van Waeyenberge, The design and verification of MuMax3, AIP Adv. **4**, 107133 (2014).

[19] G. H. Bernstein, A. Imre, V. Metlushko, A. Orlov, L. Zhou, L. Ji, G. Csaba, and W. Porod, Magnetic QCA systems, Microelectron. J. **36**, 619 (2005).

[20] J. Leliaert, A. Vansteenkiste, A. Coene, L. Dupré, and B. Van Waeyenberge, VINAMAX: A macrospin simulation tool for magnetic nanoparticles, Med. Biol. Eng. Comput. **53**, 309 (2015).

[21] L. Breth, D. Suess, C. Vogler, B. Bergmair, M. Fuger, R. Heer, and H. Brueckl, Thermal switching field distribution of a single domain particle for field-dependent attempt frequency, J. Appl. Phys. **112**, 023903 (2012).

[22] A. Lee, Z. Liu, G. Bertotti, C. Serpico, and I. Mayergoyz, Analysis of random magnetization switching using monte carlo simulations, Physica B (Amsterdam) **435B**, 100 (2014).

[23] S. B. Rao and C. Shantha, *Numerical Methods: With Programs in BASIC, FORTRAN, PASCAL and C++* (Universities Press, Telangana, India, 2004).

[24] E. Varga, G. Csaba, G. Bernstein, and W. Porod, in *2011 11th IEEE International Conference on Nanotechnology, Portland, OR, 2011* (IEEE, New York, 2011), p. 1244.

[25] D. Carlton, B. Lambson, A. Scholl, A. Young, P. Ashby, S. Dhuey, and J. Bokor, Investigation of defects and errors in nanomagnetic logic circuits, IEEE Trans. Nanotechnol. **11**, 760 (2012).

[26] J. Nogués and I. K. Schuller, Exchange bias, J. Magn. Magn. Mater. **192**, 203 (1999).

[27] S. Kirkpatrick, C. D. Gelatt, and M. P. Vecchi, Optimization by simulated annealing, Science **220**, 671 (1983).

[28] M. Akazawa, Y. Amemiya, and N. Shibata, Annealing method for operating quantum-cellular-automaton systems, J. Appl. Phys. **82**, 5176 (1997).

[29] F. M. Spedalieri, A. P. Jacob, D. E. Nikonov, and V. P. Roychowdhury, Performance of magnetic quantum cellular automata and limitations due to thermal noise, IEEE Trans. Nanotechnol. **10**, 537 (2011).

[30] A. Koppel, V. Ganesan, A. Wickenden, W. Nothwang, R. Proie, and B. Sadler, U.S. Army Research Laboratory Report No. ARL-TR-5959, 2012.